DRAFT VERSION FEBRUARY 2, 2008
Preprint typeset using LaTeX style emulateapj v. 04/03/99

arXiv:astro-ph/0305574v2 29 Jul 2003

DISCOVERY OF A NEW PULSAR WIND NEBULA IN THE LARGE MAGELLANIC CLOUD

B. M. GAENSLER[1], S. P. HENDRICK[2], S. P. REYNOLDS[1,2] AND K. J. BORKOWSKI[2]

Draft version February 2, 2008

ABSTRACT

We present new high-resolution radio and X-ray observations of the supernova remnant (SNR) B0453–685 in the Large Magellanic Cloud, carried out with the Australia Telescope Compact Array and the *Chandra X-ray Observatory* respectively. Embedded in the SNR shell is a compact central nebula producing both flat-spectrum polarized radio emission and non-thermal X-rays; we identify this source as a pulsar wind nebula (PWN) powered by an unseen central neutron star. We present a new approach by which the properties of a SNR and PWN can be used to infer upper limits on the initial spin period and surface magnetic field of the unseen pulsar, and conclude that this star was an initial rapid rotator with current properties similar to those of the Vela pulsar. As is the case for other similarly-aged sources, there is currently an interaction taking place between the PWN and the SNR's reverse shock.

Subject headings: ISM: individual (B0453–685) — supernova remnants — Magellanic Clouds

1. INTRODUCTION

The Magellanic Clouds are ideal regions for studying supernova remnants (SNRs), the known distance and low extinction obviating many of the frustrations associated with studying Galactic SNRs. While this has proved useful in studying the shell emission produced by the interaction of SNRs with the ambient medium, just two Magellanic SNRs, B0540–693 (Manchester, Staveley-Smith, & Kesteven 1993) and N157B (Wang et al. 2001), are known to harbor a young energetic pulsar and its surrounding pulsar wind nebula (PWN). The lack of other PWNe in the Magellanic Clouds is likely due to a lack of spatial resolution — such resolution is only now being applied to Magellanic SNRs in both the radio and X-ray bands, and so the prospects are good for identifying new "composite" SNRs, containing both outer shells and central PWNe. Such sources are of particular interest, as the shell and PWN together provide unique constraints on the properties of the system.

We here present data which demonstrate that B0453–685 in the LMC is a composite SNR. This *Letter* primarily discusses the central PWN; interpretation of the surrounding shell will be the focus of a subsequent paper (Hendrick et al. 2003).

2. OBSERVATIONS AND RESULTS

Radio observations of B0453–685 were carried out with the Australia Telescope Compact Array (ATCA). Observations were made simultaneously at 1.4 and 2.4 GHz with a bandwidth of 128 MHz at each frequency, using the 1.5G[3] and 6.0C configurations on 2002 Jul 23 and 2002 Aug 26 respectively. A 38.6-ks X-ray observation of the same field was carried out using the ACIS-S3 detector of the *Chandra X-ray Observatory* on 2001 Dec 18.

For each radio observation, the time on source was $\sim$11 hr. Antenna gains and polarization leakages were calibrated using observations of PKS B0252–712, while the flux density scale was tied to PKS B1934–638. The radio data were edited, calibrated and imaged using standard techniques;[4] the resulting resolution at each frequency is listed in Table 1.[5] Analysis of the *Chandra* data will be reported elsewhere (Hendrick et al. 2003).

2.1. *Imaging and Polarimetry*

Radio and X-ray images of SNR B0453–685 are shown in Figure 1. At radio frequencies, the source is clearly resolved into two components: a bright central core, embedded in an approximately circular limb-brightened shell. Table 1 lists the flux densities of these two components at 1.4 and 2.4 GHz after applying a correction for the local background. Fitting an ellipse to the perimeter of the shell component, we find that if one excludes the bright protrusion to the southwest, the shell can be fitted by a circle of diameter $120'' \pm 4''$, centered at RA (J2000) $04^{\rm h}53^{\rm m}37\overset{\rm s}{.}2$, Decl. (J2000) $-68^\circ29'30''$ (with an uncertainty $\pm 2''$). For a distance $50d_0$ kpc, the diameter of the shell is $(29 \pm 1)d_0$ pc.

Figure 2 shows that the central radio core is elongated along a position angle $\sim 45^\circ$, with dimensions $30'' \times 20''$ (i.e. a spatial size $7.3d_0$ pc $\times$ $4.8d_0$ pc). The core is brightest in the NE, where it is dominated by a slightly extended region, with peak position (J2000) RA $04^{\rm h}53^{\rm m}38\overset{\rm s}{.}6$, Dec. $-68^\circ29'21\overset{''}{.}7$ ($\pm 0\overset{''}{.}5$ in each coordinate). The core shows significant linear polarization, of mean fractional intensity 6% at 1.4 GHz and 8% at 2.4 GHz, as shown in Figure 2. The brightest region of the core is offset from the center of the shell by $11'' \pm 2''$. To the SW, the surface brightness of the core fades with increasing distance from the peak.

The third panel of Figure 1 demonstrates that the morphology of B0453–685 in the soft X-ray band shows a broadly similar structure to that seen in the radio, again revealing a central core within a limb-brightened shell. In the hard X-ray band (lower panel of Fig 1), only the central core is visible. The extent of this region is $14'' \times 7''$ ($3.4d_0$ pc $\times$ $1.7d_0$ pc), less than half that seen in the radio. Figure 2 demonstrates that the positions of the

[1]Harvard-Smithsonian Center for Astrophysics, 60 Garden Street MS-6, Cambridge, MA 02138; bgaensler@cfa.harvard.edu

[2]Department of Physics, North Carolina State University, Raleigh, NC 27695

[3]1.5G is a non-standard ATCA configuration, and has successive spacings between the six antennas of 30.6, 535.7, 306.1, 413.3 and 3015.3 meters.

[4]See `http://www.atnf.csiro.au/computing/software/miriad`.

[5]The 1.4-GHz image was formed using all antennas, while the 2.4-GHz image excluded the 6th antenna so as to not overresolve the source.

peak emission in the X-ray and radio cores coincide to within the resolution of the observations.

2.2. *Spectral Analysis*

We have carried out a spectral index study of the radio data by smoothing the 1.4 and 2.4 GHz images to a common resolution of $15''$ and then applying spectral tomography to these maps (Katz-Stone & Rudnick 1997). We find that the central core has a flatter radio spectrum than the surrounding shell: tomography implies $\alpha = -0.10 \pm 0.05$ for the core and $\alpha = -0.5 \pm 0.1$ for the shell ($S_\nu \propto \nu^\alpha$). Assuming $\alpha = -0.10$ for the core between 10^7 and 10^{11} Hz, the radio luminosity of this component is $L_R \sim 2 d_0^2 \times 10^{34}$ ergs s^{-1}.

At X-ray energies, we have determined the spectral properties of the different components of the SNR by extracting events from appropriate source and background regions and fitting to the resulting spectra, as will be described in detail by Hendrick et al. (2003). To briefly summarize their results, the shell component is well-fitted by the absorbed thermal spectrum expected in the Sedov phase of SNR evolution, while the central core is best fit by an absorbed power law.[6] The best-fit parameters for the core are a foreground absorbing column $N_H = (1.3 \pm 0.2) \times 10^{21}$ cm^{-2}, a spectral index $\alpha = -0.9 \pm 0.4$ and an unabsorbed flux density at 1 keV $f_X = (6 \pm 1) \times 10^{-14}$ erg cm^{-2} s^{-1} keV^{-1} (uncertainties quoted at 90% confidence). The corresponding X-ray luminosity over the energy range 0.5–10 keV is $L_X \sim 6 d_0^2 \times 10^{34}$ erg s^{-1}. The spectral fits for the surrounding shell imply an age $\tau \approx 13$ kyr, a swept-up mass $M_{sw} \approx 280 M_\odot$, an upstream density $n_0 \approx 0.4$ cm^{-3} and an initial explosion energy $E_0 \approx 5 \times 10^{50}$ ergs (Hendrick et al. 2003).

3. DISCUSSION

The core embedded in B0453–685 is centrally located, polarized, has a filled-center morphology and a flat radio spectrum, and is coincident with a smaller non-thermal X-ray nebula. These properties demonstrate that B0453–685 is a composite SNR, containing a synchrotron-emitting PWN powered by a neutron star embedded in a shell SNR.

3.1. *Properties of the Central Pulsar*

Within the core, no radio or X-ray point source corresponding to the central pulsar is apparent. We can calculate upper limits on the flux from such a source as follows. At radio wavelengths, we made images of the field using only the longest (> 3000 meters) five baselines in each configuration. At both 1.4 and 2.4 GHz, the brightest region of the core was still detected in these images. At the peak of nebular emission, the corresponding upper limit on a point source is 3 mJy and 0.4 mJy at 1.4 and 2.4 GHz, respectively.

In the X-ray band, we employed the SHERPA package to carry out a 2D fit to the nebular morphology. We fit the core with three components: an elliptical gaussian to define the overall shape, an unresolved source to represent an embedded pulsar, and a constant offset to account for background. Using these three components, we find that in the energy range 0.3–10 keV, the best-fit model contains 58 counts in an unresolved central source. While the apparent significance of this source seems high, we obtained equally good or better fits by replacing the unresolved component by a resolved Gaussian. This suggests a complex PWN morphology and only marginal evidence for a point source. Therefore, in subsequent discussion we adopt 58 counts as an upper limit, corresponding to a count-rate $< 1.5 \times 10^{-3}$ cts sec^{-1}. Assuming a column density $N_H = 1.3 \times 10^{21}$ cm^{-2} and a power law spectrum with a photon index $\Gamma = 1.5$ (typical for a young pulsar), this corresponds to an unabsorbed X-ray luminosity (0.5–10 keV) $L_X < 6 d_0^2 \times 10^{33}$ ergs s^{-1}.

These radio and X-ray upper limits on emission from a central pulsar are not especially constraining. Our radio limit is ~ 40 times above the upper limit for radio pulsations at this position from the survey of Manchester et al. (2003). Several young pulsars have been recently identified with a point-source X-ray luminosity $L_X \approx 10^{32} - 10^{33}$ ergs s^{-1} (Murray et al. 2002; Hughes et al. 2003), well below the limit seen here.

In the absence of a direct detection, a first guess as to the properties of the pulsar in B0453–685 can come from comparison with other systems. There are ~ 20 other shell SNRs known to contain a central X-ray/radio PWN; of these other sources, the properties of B0453–685 most closely resemble those of the Vela SNR and of G0.9+0.1, as demonstrated in Table 2. The similarity of these three systems argues that SNR B0453–685 is most likely powered by a "Vela-like" pulsar (e.g. Kramer et al. 2003), with a spin-period $P \sim 100$ ms, a surface magnetic field $B \sim 3 \times 10^{12}$ G and a spin-down luminosity $\dot{E} \approx 10^{37}$ ergs s^{-1}.

In cases in which a PWN has no identified pulsar, considerable further effort has been invested to infer the pulsar's properties (i.e. current spin period P, initial period P_0, period derivative $\dot{P}$ and surface magnetic field B) from those of its PWN. The age, spin-down luminosity and surface magnetic field of the system are, respectively:

$$\tau = \frac{P}{(n-1)\dot{P}}\left[1 - \left(\frac{P_0}{P}\right)^{n-1}\right], \quad \dot{E} = 4\pi^2 I \frac{\dot{P}}{P^3}, \quad B = 3.2 \times 10^{19} (P\dot{P})^{1/2} \text{ Gauss}, \tag{1}$$

where $I \equiv 10^{45}$ g cm^2 is the star's moment of inertia, $n \equiv 2 - P\ddot{P}/\dot{P}^2$ is the "braking index", and P is in seconds. Typically one assumes $n = 3$, $P_0 = 0$ and $L_X = \eta \dot{E}$ (where η is an assumed efficiency factor). L_X and τ are determined from observations, from which estimates for P, $\dot{P}$ and B can then be derived using Equations (1).

Here we propose an alternative approach, where rather than assuming an (unphysical) value of P_0, we use the above expressions to eliminate P and $\dot{P}$, and thus obtain a relation between B and P_0. Assuming that B is constant with time, the resulting function has absolute maxima in both B and P_0. The robust upper limits on the surface magnetic field and the initial spin period of the neutron star which result are:

$$B < 3.2 \times 10^{19} \frac{U}{\tau(n-1)} \text{ Gauss}; \quad P_0 < U(\tau[n+1])^{-1/2} \left(\frac{2}{n+1}\right)^{\frac{1}{n-1}}, \tag{2}$$

where $U^2 = P^3/\dot{P} = 4\pi^2 I \eta / L_X$. These limits are reasonably insensitive to the value of n assumed; for $2 < n < 3$ (encompassing the range for the four pulsars for which n has been directly measured; e.g. Cusumano, Massaro, & Mineo 2003), we find $B < (3.1 - 6.3)\eta^{1/2} \times 10^{13}$ G and $P_0 < (448 - 488)\eta^{1/2}$ ms for this system. For other PWNe, a solid upper limit is $\eta < 0.05$; we have argued above that the pulsar here is "Vela-like", for which $\eta \approx 0.01 - 0.001$ is more reasonable (Possenti et al. 2002).

[6] Bremsstrahlung ($kT \sim 4$ keV) can also fit the central core, but the absence of lines demands either absurdly low abundances or an extremely underionized plasma (ionization timescale $n_e t < 100$ yr cm^{-3}).

We thus conclude that this pulsar has a surface magnetic field $B < 6 \times 10^{12}$ G and an initial spin period $P_0 < 50$ ms. These values are consistent with "typical" radio pulsars such as the Crab ($B = 4 \times 10^{12}$ G, $P_0 = 19$ ms) and Vela ($B = 3 \times 10^{12}$ G) pulsars, but not with the emerging class of young pulsars which are highly magnetized and/or slow initial rotators, such as PSRs J1846–0258 ($B = 5 \times 10^{13}$ G; Gotthelf et al. 2000) or J1210–5226 ($P_0 \approx 400$ ms; Pavlov et al. 2002).

3.2. *Evolutionary State of the PWN*

Chevalier (1998) divides PWN evolution into successive phases. The PWN first expands supersonically in the SNR interior. The PWN then collides with the SNR reverse shock; this compresses the PWN and causes it to expand more slowly. The pulsar's motion can later become supersonic in the shocked SNR interior, and it then drives a bow-shock.

If we assume that the pulsar spin-down luminosity is constant in the initial supersonically expanding phase, the radius of the PWN evolves such that $R_{PWN} = 0.839 \times (\dot{E}\tau/E_0)^{1/5} V_0 \tau$, where V_0 was the initial expansion velocity of the SNR (van der Swaluw et al. 2001). Here we observe $R_{PWN} \approx 3$ pc, $\tau \approx 13$ kyr and $E_0 \approx 5 \times 10^{50}$ ergs, and we adopt $\dot{E} = E_{37} \times 10^{37}$ ergs s^{-1}. Thus if the PWN is still in this phase of evolution, we require $V_0 \approx 700 E_{37}^{-1/5}$ km s^{-1}, implying an enormous ejected mass $M_{ej} = 2E_0/V_0^2 \approx 100 E_{37}^{2/5}\, M_\odot$. We thus conclude that the PWN is almost certainly not expanding supersonically, having a radius much smaller than expected in this interpretation.

The brightest radio and X-ray emission from the PWN is offset from the SNR's geometric center by $l = (2.7 \pm 0.5) d_0$ pc. Since this peak most likely marks the current position of the unseen pulsar, a possible interpretation is that the pulsar is moving away from its birth site with a transverse velocity $V_T = l/\tau = 200 \pm 40$ km s^{-1}. The radio PWN is clearly elongated, with a fading tail pointing back along the implied direction of motion. While this is suggestive of a bow shock morphology, this requires that the pulsar be moving supersonically through shocked ejecta. In the Sedov solution, this condition is met only when $l/R_{SNR} \gtrsim 0.7$ (van der Swaluw, Achterberg, & Gallant 1998). Unless the pulsar's motion is at less than $\sim 20^\circ$ to the line-of-sight (implying a true velocity $V > 700$ km s^{-1}), the pulsar in this system is still too close to the center of its SNR to meet this requirement.

The remaining possibility is that this PWN has undergone a reverse shock interaction with its SNR, and is now expanding subsonically. Such an interaction begins at an age ~ 10 kyr when $M_{sw} \gtrsim 10\, M_{ej}$ (Chevalier 1998), consistent with the properties of this source. The elongated morphology and comparatively small radius seen for the radio PWN are simply accounted for by reverse-shock compression; the same properties have been similarly interpreted in the other SNRs listed in Table 2 (Blondin, Chevalier, & Frierson 2001).

4. CONCLUSIONS

New radio and X-ray observations of SNR B0453–685 in the LMC demonstrate this source to consist of both an outer shell and a central pulsar-powered nebula. We have used the properties of this SNR to infer that the unseen central engine is a typical young radio pulsar, with an initial period $P_0 < 50$ ms, a current period $P \sim 100$ ms, a surface field $B < 6 \times 10^{12}$ G and a spin-down luminosity $\dot{E} \sim 10^{37}$ erg s^{-1}. The small and elongated radio nebula results from compression of the PWN by the SNR reverse shock.

This study demonstrates that several useful constraints on the properties of an unseen pulsar can be inferred from those of its associated PWN and SNR, provided that good estimates for the system's distance and age are available. With many new studies of PWNe and composite SNRs now emerging, such an approach can be applied to many other sources.

We thank Bob Sault for allowing us to carry out the ATCA observations remotely from Harvard University, Dick Manchester for information on pulsar surveys of the LMC, and Eric van der Swaluw and Patrick Slane for useful discussions. The Australia Telescope is funded by the Commonwealth of Australia for operation as a National Facility managed by CSIRO. This work was supported by NASA through grants GO1-2075X and NAG5-13032.

REFERENCES

Blondin, J. M., Chevalier, R. A., & Frierson, D. M. 2001, ApJ, 563, 806.
Chevalier, R. A. 1998, Mem. della Soc. Ast. It., 69, 977.
Cusumano, G., Massaro, E., & Mineo, T. 2003, A&A, 402, 647.
Gotthelf, E. V., Vasisht, G., Boylan-Kolchin, M., & Torii, K. 2000, ApJ, 542, L37.
Helfand, D. J. & Becker, R. H. 1987, ApJ, 314, 203.
Helfand, D. J., Gotthelf, E. V., & Halpern, J. P. 2001, ApJ, 556, 380.
Hendrick, S. P. et al. 2003, in preparation.
Hughes, J. P., Slane, P. O., Park, S., Roming, P. W. A., & Burrows, D. N. 2003, ApJ, 591, L139.
Katz-Stone, D. M. & Rudnick, L. 1997, ApJ, 488, 146.
Kramer, M. et al. 2003, MNRAS, in press (astro-ph/0303473).
Manchester, R. N., Fan, G., Lyne, A. G., Kaspi, V. M., & Crawford, F. 2003, in preparation.
Manchester, R. N., Staveley-Smith, L., & Kesteven, M. J. 1993, ApJ, 411, 756.
Murray, S. S., Slane, P. O., Seward, F. D., Ransom, S. M., & Gaensler, B. M. 2002, ApJ, 568, 226.
Pavlov, G. G., Zavlin, V. E., Sanwal, D., & Trümper, J. 2002, ApJ, 569, L95.
Porquet, D., Decourchelle, A., & Warwick, R. S. 2003, A&A, 401, 197.
Possenti, A., Cerutti, R., Colpi, M., & Mereghetti, S. 2002, A&A, 387, 993.
van der Swaluw, E., Achterberg, A., & Gallant, Y. A. 1998, Mem. della Soc. Ast. It., 69, 1017.
van der Swaluw, E., Achterberg, A., Gallant, Y. A., & Tóth, G. 2001, A&A, 380, 309.
Wang, Q. D., Gotthelf, E. V., Chu, Y.-H., & Dickel, J. R. 2001, ApJ, 559, 275.
Weiler, K. W. & Panagia, N. 1980, A&A, 90, 269.

TABLE 1
RADIO PROPERTIES OF SNR B0453–685.

Waveband (cm)	Resolution (arcsec)	Flux Density (mJy) Core	Shell	Total
1.4 GHz	7.3×6.7	46 ± 2	140 ± 2	186 ± 3
2.4 GHz	9.2×8.4	46 ± 2	105 ± 2	151 ± 3

TABLE 2
COMPARISON OF SNR B0453–685 TO OTHER SIMILAR SYSTEMS.

SNR	Age (10^3 yr)	R_{SNR} (pc)	R_{PWN}	$L_{R,PWN}$ (10^{34} ergs s^{-1})	$L_{X,PWN}$	Ref[b]
B0453–685	13	29 ± 1	7×5	2	6	1
Vela SNR	~ 11	42	10	0.8	0.8[a]	2, 3
G0.9+0.1	$\sim 10-20$	20	6	7	6	4, 5

R_{SNR} and R_{PWN} are the radii of the SNR and PWN respectively; $L_{R,PWN}$ and $L_{X,PWN}$ are the approximate radio and X-ray luminosities, respectively, of the PWN.
[a] The PWN luminosity quoted by Helfand et al. (2001) is much lower than this, but corresponds to only the innermost component of the PWN.
[b] REFERENCES: (1) This paper; (2) Weiler & Panagia (1980); (3) Helfand et al. (2001); (4) Helfand & Becker (1987); (5) Porquet et al. (2003).

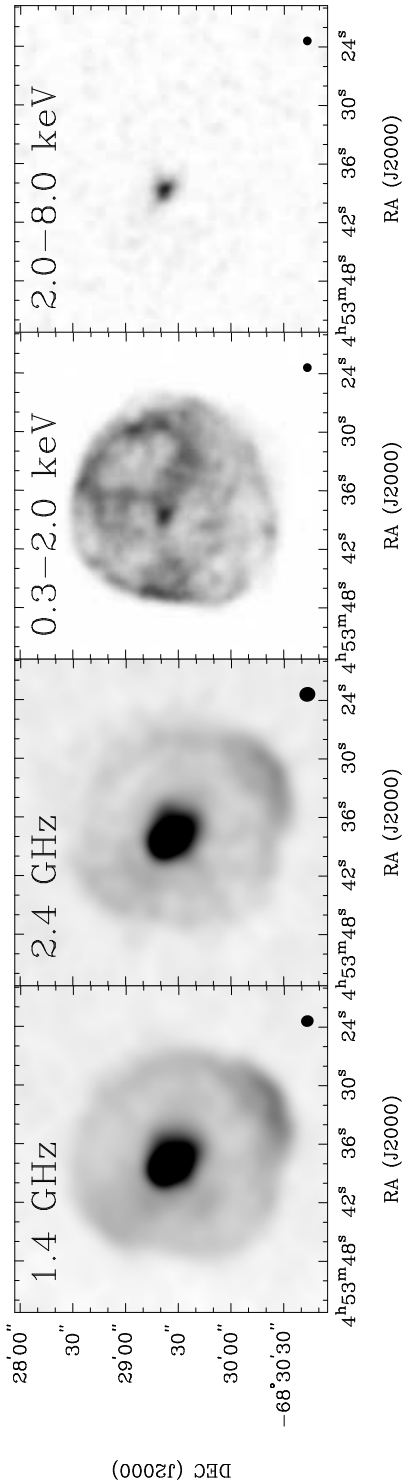

FIG. 1.— Radio and X-ray images of SNR B0453–685. The top two panels show ATCA radio images of the source at 1.4 and 2.4 GHz, while the bottom two panels show *Chandra* X-ray images of B0453–685 in the soft and hard bands. The two radio images have both been smoothed to a resolution of $10'' \times 10''$. The sensitivity of the radio images are 95 and 65 μJy beam^{-1} at 1.4 and 2.4 GHz respectively. Both radio images are shown over the same greyscale range, –0.4 to +5.7 mJy beam^{-1}. The X-ray images have both been smoothed with a gaussian of FWHM $5'' \times 5''$; the greyscale ranges are 0%–100% and 0%–56% of the peak for the soft- and hard-band images respectively. In all four panels, the point-spread function is shown by the ellipse in the lower-right corner, and the greyscale is shown using a linear transfer function.

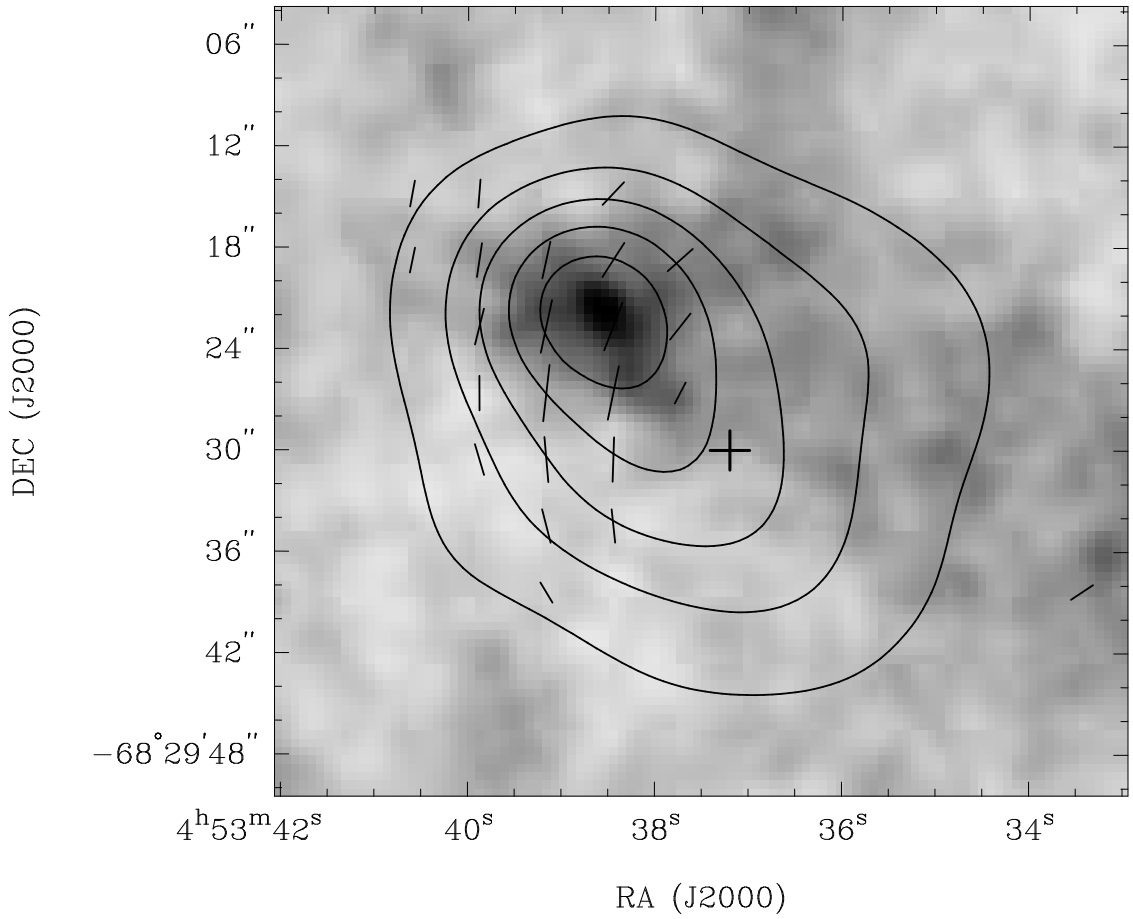

FIG. 2.— Radio and X-ray images of the core of SNR B0453–685. The greyscale shows X-ray emission from the central region of B0453–685 as seen by *Chandra* in the energy range 0.3–8.0 keV, smoothed to a resolution of 2″. The contours represent the 2.4-GHz image at full resolution (9.″2 × 8.″4), drawn at the levels of 2, 4, 6, 8 and 10 mJy beam^{-1}; the rms sensitivity of these data are 70 μJy beam^{-1}. Overlaid as vectors are the 2.4-GHz linearly polarized intensity at each position; the length of each vector is proportional to the polarized intensity (up to a maximum of 0.7 mJy beam^{-1}) and the orientation of the vector indicates the mean position angle of the electric field (averaged across the observing bandwidth, and not corrected for Faraday rotation). The "+" symbol indicates the center fitted for the surrounding SNR shell.